Neuron
Article

Reciprocal Inhibition of Inhibition: A Circuit Motif for Flexible Categorization in Stimulus Selection

Shreesh P. Mysore[1,*] and Eric I. Knudsen[1]
[1]Department of Neurobiology, Stanford University, 299 W. Campus Drive, Stanford, CA 94305, USA
*Correspondence: shreesh@stanford.edu
DOI 10.1016/j.neuron.2011.10.037

SUMMARY

As a precursor to the selection of a stimulus for gaze and attention, a midbrain network categorizes stimuli into "strongest" and "others." The categorization tracks flexibly, in real time, the absolute strength of the strongest stimulus. In this study, we take a first-principles approach to computations that are essential for such categorization. We demonstrate that classical feedforward lateral inhibition cannot produce flexible categorization. However, circuits in which the strength of lateral inhibition varies with the relative strength of competing stimuli categorize successfully. One particular implementation—reciprocal inhibition of feedforward lateral inhibition—is structurally the simplest, and it outperforms others in flexibly categorizing rapidly and reliably. Strong predictions of this anatomically supported circuit model are validated by neural responses measured in the owl midbrain. The results demonstrate the extraordinary power of a remarkably simple, neurally grounded circuit motif in producing flexible categorization, a computation fundamental to attention, perception, and decision making.

INTRODUCTION

The segregation of continuously varying stimuli into discrete, behaviorally relevant groups, a process referred to as categorization, is central to perception, stimulus identification, and decision making (Freedman and Assad, 2006; Freedman et al., 2001; Leopold and Logothetis, 1999; Niessing and Friedrich, 2010). In some cases, the boundary between categories is fixed (Prather et al., 2009). In most cases, however, the boundary needs to adjust according to context, a process referred to as flexible categorization. Recent research suggests that such flexible categorization also contributes to competitive stimulus selection for gaze and attention (Mysore and Knudsen, 2011b). A midbrain network that plays an essential role in gaze and attention (Cavanaugh and Wurtz, 2004; Lovejoy and Krauzlis, 2010; McPeek and Keller, 2004; Müller et al., 2005) segregates stimuli into "strongest" and "others" (Mysore and Knudsen, 2011a). The midbrain network includes the optic tectum (called the superior colliculus in mammals) and several nuclei in the midbrain tegmentum, referred to as the isthmic nuclei (Knudsen, 2011). Categorization by this network tracks the location of the strongest stimulus in real time as a precursor to the selection of the next target for gaze and attention. Despite the importance of flexible categorization to a broad range of functions, how the brain implements it is not known.

Categorization by the midbrain network arises from special response properties of a subset of neurons located in the intermediate and deep layers of the owl optic tectum (OTid) (Mysore et al., 2011; Mysore and Knudsen, 2011a). These neurons display "switch-like" responses, firing at a high rate when the stimulus inside their classical receptive field (RF) is the strongest (highest intensity or speed) but switching abruptly to a lower firing rate when a distant, competing stimulus becomes the strongest. This switch-like property causes the encoding of categories by the OTid to be explicit: the category can be read out directly from the population activity pattern without any further transformations beyond simple linear operations, such as averaging (Gollisch and Meister, 2010). In addition, if the strength of the stimulus inside the RF is increased, a switch-like neuron requires a correspondingly stronger competing stimulus to suppress its responses. This property causes the category boundary to be flexible, enabling network responses to reliably identify the strongest stimulus at each moment in time. Explicit and flexible categorization by this network dramatically improves the discriminability of the strongest stimulus among multiple competing stimuli of similar strength (Mysore et al., 2011; Mysore and Knudsen, 2011a).

The properties of stimulus categorization exhibited by neurons in the owl OTid account well for behavioral deficits in monkeys following the inactivation of the intermediate and deep layers of the superior colliculus (Lovejoy and Krauzlis, 2010; McPeek and Keller, 2004; Nummela and Krauzlis, 2010). In monkeys performing stimulus selection tasks, focal inactivation of the portion of the superior colliculus representing the target stimulus causes an impairment in their ability to select an oddball target or a spatially cued target among distracters, an impairment that increases dramatically as the distracting stimuli become more similar to the target stimulus. These studies indicate that the midbrain network performs computations that are essential for reliable competitive stimulus selection, especially when competing stimuli are of similar strength.

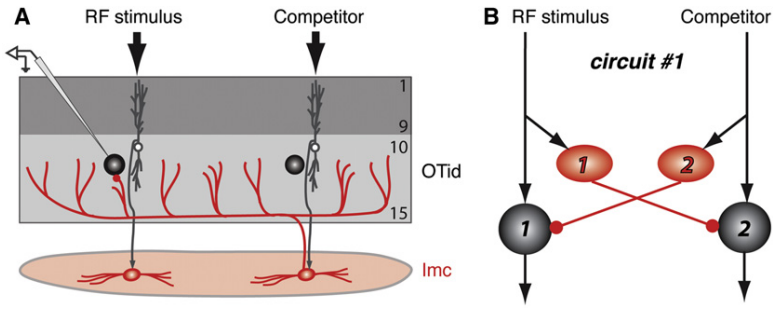

Figure 1. Feedforward Lateral Inhibition to the OTid

(A) Key elements of the midbrain network: the superficial layers of the optic tectum (layers 1–9), the intermediate and deep layers of the optic tectum (OTid), and a GABAergic nucleus in the midbrain tegmentum, the Imc. Space-specific excitation due to a stimulus (black arrows) drives neurons in both the OTid and the Imc. The Imc neurons send long-range, lateral inhibitory projections to OTid neurons coding for all other spatial locations (red line). For clarity, the projections of only one Imc neuron are shown. Consequently, unlike in sensory normalization circuits, in this circuit, a stimulus does not contribute to the suppression of its own responses.

(B) Schematic of a feedforward lateral inhibitory circuit (circuit 1) with long-range inhibitory projections from the Imc (red ovals, inhibitory units) to the OTid (black circles, output units). Black arrows indicate excitatory connections. Two out of many spatial channels in the space map are shown. One channel (1) represents the RF stimulus; the other (2) represents the competing stimulus.

A neural computation that is fundamental to stimulus competition in the OTid is the suppression of responses to an RF stimulus by stimuli located outside the RF. Such "surround suppression" is observed in many brain areas across many species (Allman et al., 1985). Unlike interactions that occur among stimuli within the RF (such as crossorientation suppression in the visual cortex; Freeman et al., 2002), surround suppression is thought to be mediated by lateral inhibition and, often, by feedforward lateral inhibition (Blakemore and Tobin, 1972; Bolzon et al., 2009; Cisek and Kalaska, 2010; Hartline et al., 1956; Kuffler, 1953; Olsen et al., 2010; Yang and Wu, 1991). Anatomical evidence from the avian midbrain network supports lateral inhibition as underlying global suppression in the OTid as well (Figure 1; Wang et al., 2004). Specifically, a midbrain GABAergic nucleus, the nucleus isthmi pars magnocellularis (Imc), receives focal input from neurons with dendrites in the retinorecipient layers of the optic tectum and sends broad projections to neurons in the multimodal and motor layers of the optic tectum, the OTid.

Through the use of this basic feedforward lateral inhibitory circuit as a starting point, we employ a first principles approach to address neural computations that underlie flexible categorization in the OTid. We show that feedforward lateral inhibition, a circuit motif at the heart of most models of selection for attention or action (Cisek and Kalaska, 2010; Lee et al., 1999), cannot account for categorization that is flexible. However, a simple modification—introducing reciprocal inhibition between feedforward lateral inhibitory channels—successfully achieves flexible categorization. The key additional computation that achieves adaptive boundary flexibility in categorization is lateral inhibition that is dependent on relative stimulus strength. Reciprocal inhibition of feedforward lateral inhibition emerges as an extremely simple yet powerful motif that implements this computation rapidly and reliably, thereby producing flexible categorization, a process central to attention, perception, and decision making (Freedman and Assad, 2011).

RESULTS

To identify neural circuits that might achieve categorization, we began by first capturing basic properties of neuronal responses to single and multiple competing stimuli. To this end, we use standard mathematical equations that account accurately for experimental results and that have been employed widely in the literature.

Responses of the OTid to Single Stimuli Are Nonlinear

OTid neurons respond nonlinearly to increasing strengths of a single stimulus inside their RFs. Strong stimuli (high contrast, high-sound level, fast motion, etc.) drive neurons to saturation. These nonlinear responses are well fit by sigmoidal functions (Mysore et al., 2010, 2011). In this study, looming visual stimuli (expanding dots) were used to drive neural responses. A standard sigmoidal equation, the hyperbolic-ratio function (Naka and Rushton, 1966), describes OTid responses to an RF stimulus of loom speed l:

$$OT = a + b\left(\frac{l^n}{l^n + L_{50}^n}\right) \quad (1)$$

The parameters are a, the minimum response; b, the maximum change in response; L_{50}, the loom speed that yields a half-maximum response; and n, a factor that controls response saturation. The mechanisms that underlie response saturation to single stimuli are distinct from those that mediate global surround suppression, the focus of this study (Freeman et al., 2002; Mysore et al., 2010). Therefore, without loss of generality, we focus on the lateral inhibition for surround suppression while using the sigmoidal function as a description of OTid responses to single stimuli.

For subsequent simulations, the best sigmoidal fit to the experimentally measured, average loom speed-response function from 61 OTid neurons (Figure 2A) was used as the response function of a typical OTid unit:

$$OT = 5.3 + 22.2\left(\frac{l^2}{l^2 + 11.6^2}\right) \quad (2)$$

Here, the first term (5.3) represents the contribution of the contrast of a stationary dot (loom speed = 0°/s) to the response: the average response to a loom speed of 0°/s at full contrast was 5.3 sp/s. Because this contribution of stimulus contrast was small, we made the simplifying assumption that the dependence of the response on the contrast of a stationary dot was linear. Because all responses were simulated for full-contrast

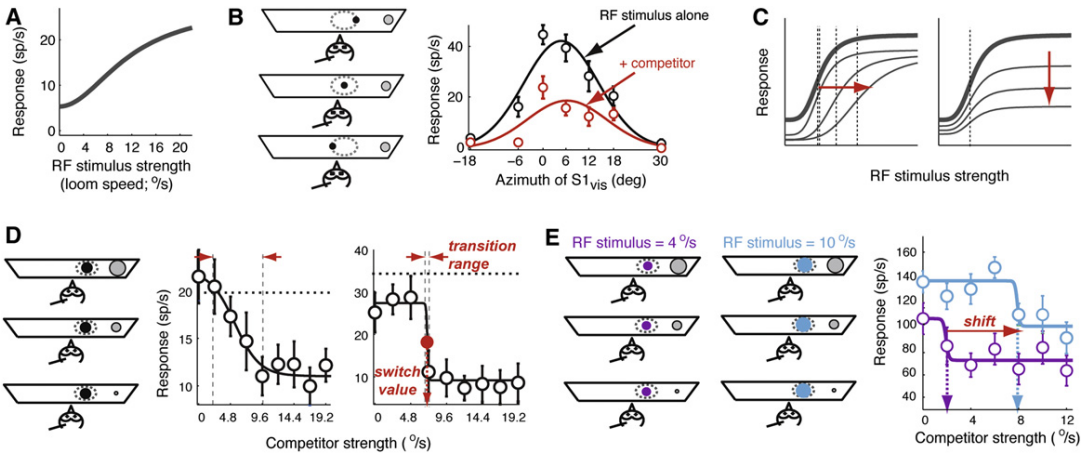

Figure 2. Neuronal Response Properties and Signatures of Explicit, Flexible Categorization in the Owl OTid

(A) Strength-response function of a typical OTid unit. Curve represents the average loom speed-response function for a single looming stimulus centered in the RF, computed from 61 OTid neurons.

(B) Distant competitor produces divisive suppression of spatial tuning curves in the OTid. Left: stimulus protocol. Dashed ovals indicate RF, black dots indicate RF stimulus, and gray dots indicate competitor located outside the RF, 30° away. The sizes of the dots represent the strengths (loom speeds) of the stimuli. Note that in experiments, both stimuli were always full-contrast dark dots on a light background. Right: black curve indicates azimuthal tuning curve with RF stimulus alone, and red curve indicates tuning curve measured in the presence of a competitor, which produces divisive response suppression.

(C) Effect of divisive influences on stimulus strength-response functions. Red arrows indicate increasing strength of inhibition. Dashed vertical lines represent half-maximum response strengths. Left: effect of input division. Right: effect of output division.

(D) Competitor strength-response profiles (CRPs) measured with competing looming visual stimuli. Left: stimulus protocol. Dashed ovals indicate RF, black dots indicate RF stimulus, and gray dots indicate competitor located outside the RF, 30° away. Strength of the RF stimulus is held constant, whereas that of the competitor is systematically varied. The sizes of the dots represent the strengths (loom speeds) of the stimuli. Middle: a CRP showing a gradual, nonlinear increase in response suppression, with increasing strength of the competitor. RF stimulus strength = 7.2°/s. Horizontal dotted line indicates responses to RF stimulus alone. Vertical dashed lines indicate the transition range (7.5°/s). Right: a switch-like CRP showing an abrupt increase in response suppression, with increasing strength of the competitor over a narrow range. RF stimulus strength = 8°/s. Horizontal dotted line indicates responses to RF stimulus alone. Vertical dashed lines indicate the transition range (0.4°/s). Red dot and arrows indicate the switch value (7.2°/s).

(E) Adaptive shift in the switch values of CRPs with changes in RF stimulus strength. Left: stimulus protocol. The two sets of stimuli were presented in an interleaved fashion. Right: the CRP measured with the stronger RF stimulus (blue) is shifted rightward with respect to the CRP measured with the weaker RF stimulus (magenta).

For (B), (D), and (E), error bars indicate SEM. All panels are adapted from Mysore et al. (2010, 2011). See also Figure S1.

stimuli (contrast = 1), the contrast-related term was simply a constant, 5.3.

Lateral Inhibition Is Divisive and Scales Nonlinearly with Competitor Strength

Responses to RF stimuli are divisively suppressed by a competing stimulus located outside the RF (Figure 2B; Mysore et al., 2010). We captured this divisive effect of lateral inhibition by introducing both input and output divisive influences in a manner similar to previously published reports (Equation 3; Olsen et al., 2010).

$$OT = \left(\frac{1}{s_{out}+1}\right)\cdot\left(\frac{5.3}{s_{in}+1}+22.2\left(\frac{I^2}{I^2+11.6^2+s_{in}^2}\right)\right) \quad (3)$$

Here, s_{in} and s_{out} are suppressive factors that produce input and output division, respectively (see Supplemental Experimental Procedures available online).

Experiments in the OTid have demonstrated that response inhibition increases as the strength of the competitor increases and does so, typically, in a nonlinear (sigmoidal) manner (Figure 2D; Mysore et al., 2011). To incorporate competitor strength-dependent inhibition, we took the suppression factors s_{in} and s_{out} to be proportional to the activity I of the inhibitory units driven by stimuli located outside the RF:

$$s_{in} = d_{in}\cdot I, s_{out} = d_{out}\cdot I \quad (4)$$

where d_{in} and d_{out} were proportionality constants, and I was the inhibitory activity driven by the competitor. Recordings of Imc responses to single looming stimuli have shown that they are well fit by sigmoidal functions (S.M., unpublished data). Consequently, inhibitory activity as a function of the loom speed of the competitor stimulus was modeled as having the same form as Equation 1:

$$I = m + h\left(\frac{I^k}{I^k+s_{50}^k}\right) \quad (5)$$

The free parameters were m, the minimum response; h, the maximum change in response; S_{50}, the loom speed that yields a half-maximum response; and k, a factor that controls response saturation. The effect of changing the values of each of these parameters on I is illustrated in Figure S1. A linear dependence between the input and output divisive factors (s_{in} and s_{out}) and the inhibitory activity (I) was assumed in Equation 4 for simplicity. This formulation minimized the number of free parameters in the

model, while still allowing for nonlinear competitor strength-dependent response suppression, due to the nonlinearity of I.

Response Properties Essential to Explicit and Flexible Categorization in the OTid

We now describe the special response properties underlying strongest versus other categorization that need to be accounted for by the model. These were revealed in experiments in which a looming stimulus of fixed speed was presented inside the RF, while a second competing stimulus of variable speed was presented far outside the RF, about 30° away. The resulting responses are referred to as the competitor strength-response profile, or CRP (Mysore et al., 2011).

Explicit Encoding of Categories

Essential to the explicit representation of categories in the OTid is the abrupt, switch-like increase in response suppression, observed in about 30% of OTid neurons, as the strength of a competing stimulus is increased (Figure 2D, right). The abruptness of the transition is quantified as the range of competitor strengths over which CRP responses drop from 10% to 90% of the maximum change in response and is referred to as the transition range. Switch-like CRPs were defined as those for which the transition range was very narrow: $\leq 4°$/s, equivalent to $\leq 1/5$ of the full range of loom speeds tested. Population activity patterns that include switch-like responses (along with non-switch-like responses) explicitly categorize stimuli into two categories, strongest and others, as determined by crosscorrelational analysis (Mysore and Knudsen, 2011a). Conversely, excluding the top 20% of the neurons with the most abrupt response transitions (switch-like responses) from the population analysis eliminates categorization by the population activity.

Switch-like responses are not winner take all: the responses to the RF stimulus when it is weaker than the competitor, i.e., when it is the "losing" stimulus, are not driven to zero. Rather, the responses scale with the absolute strength of the losing RF stimulus (Figure 2E, right, magenta versus blue data; Figures S1E–S1I) (Mysore et al., 2011).

Flexibility of Categorization

The flexibility of categorization in the OTid requires that the boundary between categories dynamically track the strength of the strongest stimulus. For switch-like CRPs, the strength of the competitor that caused responses to drop from a high to a low level (Figure 2D, red dot), called the switch value, equaled, on average, the strength of the RF stimulus and was therefore indicative of the categorization boundary. Moreover, when two CRPs were measured for a unit using two different RF stimulus strengths, the switch value shifted with the strength of the RF stimulus (Figure 2E), and, across all tested switch-like units, the average shift in the switch value was equal to the change in the strength of the RF stimulus.

Population activity patterns constructed using these CRP responses exhibited an appropriately shifting category boundary with RF stimulus strength (Mysore and Knudsen, 2011a). Conversely, when switch-like responses were removed from the population, flexible categorization did not occur. Thus, switch-like responses and adaptive shifts in switch value with changes in RF stimulus strength are, respectively, the signatures of the explicit and flexible categorization in the OTid.

Results from Model Circuit 1: Feedforward Lateral Inhibition

We asked whether a feedforward lateral inhibitory circuit could produce the two response signatures critical for categorization in the OTid. This circuit architecture served as a good starting point, because it is anatomically supported in the midbrain network, and similar architectures have been used to model sensory processing of multiple stimuli as well as the selection of stimuli for attention and action in many different brain structures.

In the following simulations, we present the results from the perspective of output unit 1 (Figure 1B, black circle) and the inhibitory unit that suppresses it, inhibitory unit 2 (Figure 1B, red oval). Because the connections and weights are symmetrical, the results would apply to neurons representing additional spatial channels in the output or inhibitory unit layers.

Feedforward Lateral Inhibition Alone Can Produce Switch-like CRPs

To test whether this circuit model can produce switch-like CRPs at the output (OTid) units, we simulated responses with the strength of the RF stimulus held constant at 8°/s and the strength of the competitor stimulus increased systematically from 0°/s to 22°/s. We expected that any parameter that affected the steepness of the inhibitory-response function would, in turn, affect the steepness of the CRP. Therefore, increasing the saturation parameter k (Figure S1A) and decreasing the half-maximum parameter S_{50} (Figure S1B), both of which make the inhibitory-response function steeper, should yield CRPs with transition ranges narrower than 4°/s.

Consistent with these expectations, large enough values of k (Figure 3B, top left) and small enough values of S_{50} over a wide range (Figure 3B, top right) successfully produced switch-like CRPs at the output units. Based on these results, we chose the parameter values of the inhibitory-response function for subsequent simulations to be $k = 10$, $S_{50} = 8$, $m = 5$, and $h = 15$. The resulting switch-like CRP is shown in Figure 3C.

Feedforward Lateral Inhibition Cannot Produce Adaptive Shifts of CRPs

Next, we tested whether this circuit model can produce adaptive shifts in the CRP switch value. We simulated two CRPs with RF stimulus strengths of 8°/s and 14°/s, respectively, and asked whether any combination of input and output divisive inhibition (d_{in} and d_{out}, respectively; Equations 2 and 3) could appropriately shift the CRP switch value.

The ranges of d_{in} and d_{out} tested, [0, 3] and [0, 0.24], respectively, were chosen such that the smallest value produced no modulation of the RF stimulus-response function, and the largest value produced 90% of the maximum possible modulation (Figures S2A and S2B). All the parameters of the inhibitory-response function were maintained at the previous values, chosen to yield switch-like CRPs. For each pair of d_{in} and d_{out} values, we computed the switch values for the two CRPs and calculated them as the CRP shift ratio, the ratio of the shift in the switch value to the change in the RF stimulus speed; a ratio of 1 represents a perfectly adaptive shift.

The plot of model CRP shift ratios as a function of d_{in} and d_{out} demonstrated that this circuit produced almost no shift in CRP switch values in response to an increase in the strength of the

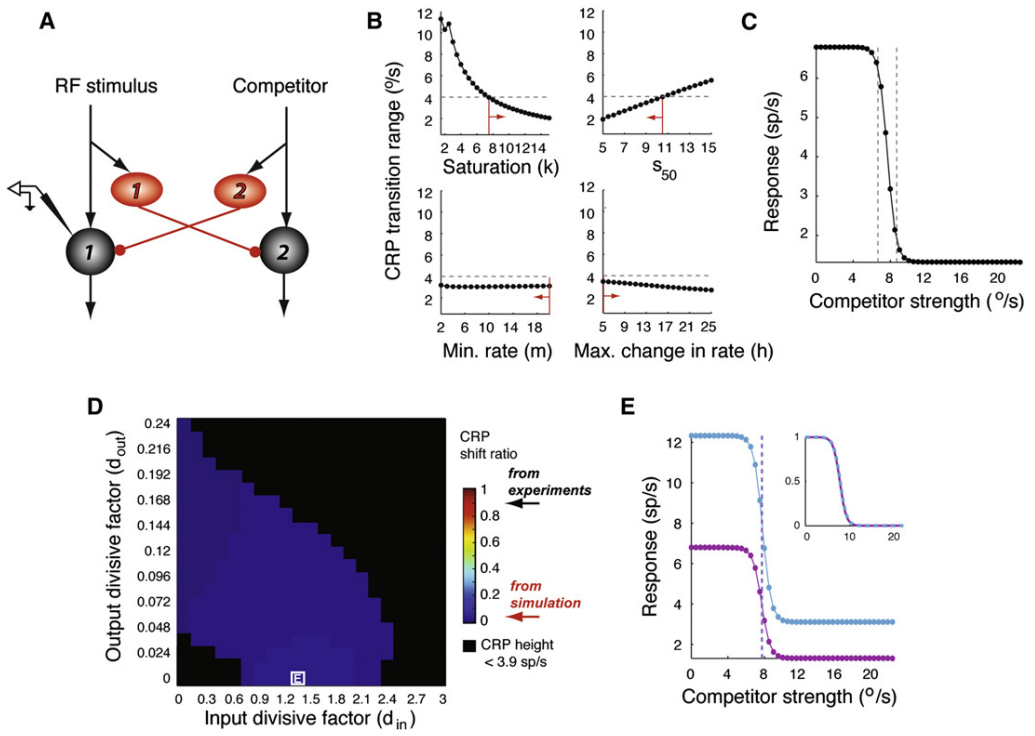

Figure 3. Feedforward Lateral Inhibition, Circuit 1, Can Produce Switch-like CRPs, but Not Adaptive Shifts in CRP Switch Value

(A) Schematic of the circuit. Recording icon indicates the unit for which responses are shown in (B) and (C).

(B) Effect of varying the parameters of the inhibitory-response function on the CRP transition range of output unit 1. Red line and arrow indicate the range of values of a parameter over which CRPs are switch like (transition ranges $\leq 4°$/s). The value of the indicated parameter was varied systematically while the other parameters were held constant at the following values: $k = 10$, $S_{50} = 8$, $m = 5$, $c = 15$, $d_{in} = 1$, and $d_{out} = 0.05$.

(C) The switch-like CRP produced at output unit 1 when the values of the parameters of the inhibitory-response function were set at $k = 10$, $S_{50} = 8$, $m = 5$, $c = 15$, $d_{in} = 1$, and $d_{out} = 0.05$.

(D) CRP shift ratio (shift in CRP switch value / change in the strength of the RF stimulus) as a function of the input and output division factors (d_{in} and d_{out}). The change in the RF stimulus strength was 6°/s (chosen to match experimental tests, Mysore et al., 2011). The black-shaded values indicate (d_{in}, d_{out}) pairs that yielded CRPs for which at least one of them had a maximum change in response smaller than the threshold of 3.9°/s (Experimental Procedures) or for which one of the CRPs was not switch-like (transition range > 4°/s). Largest value of CRP shift ratio = 0.03, obtained at the (d_{in}, d_{out}) pair = (1.5, 0), indicated by the boxed letter E. The resulting CRPs are shown in (E).

(E) The two CRPs corresponding to the (d_{in}, d_{out}) pair that yielded the largest CRP shift ratio ($d_{in} = 1.5$, $d_{out} = 0$).

See also Figure S2.

RF stimulus (Figure 3D and Figure S2C). The maximum shift ratio produced was 0.03 ($d_{in} = 1.5$, $d_{out} = 0$), and the two CRPs corresponding to this shift ratio are shown in Figure 3E.

To understand why this circuit cannot produce adaptive shifts in the CRP switch value, we compared the patterns of inhibition in the two CRP measurement conditions. Because the activity of the inhibitory neuron (I) depended only on the strength of the competitor and not on the strength of the RF stimulus (I, s_{in} and s_{out}; Equation 4), the pattern of inhibition was identical in both cases (Figure S2E; identical magenta and blue lines). Therefore, the only difference between the two CRPs measured at the output unit was the upward (without a rightward) shift (Figure 3E, blue curve relative to magenta curve), reflecting the increased excitatory drive caused by the stronger RF stimulus (I in Equation 3). The simulations for Figure 3 explored a large portion, but not the entire space, of parameter values. Nonetheless, it is clear from the above observation that no possible combination of parameters for this circuit can produce adaptive, rightward shifts in the CRP when the strength of the RF stimulus is changed.

Thus, feedforward lateral inhibition, as modeled with widely used divisive normalization (Equation 5), although able to produce switch-like CRPs, is unable to produce adaptive shifts in the CRP switch value. Therefore, it is unable to account for flexible categorization.

Model Circuit 2: Reciprocal Inhibition of Feedforward Lateral Inhibition

The results above suggest that, in order for CRP switch values to shift adaptively with changes in the strength of the RF stimulus, the strength of inhibition must depend on the relative strengths of the competitor and RF stimuli, rather than just on the strength of the competitor alone. In other words, the term I in Equation 4 must depend on relative-stimulus strength.

From a circuit perspective, the simplest modification to achieve this goal is to have the inhibitory units inhibit each other

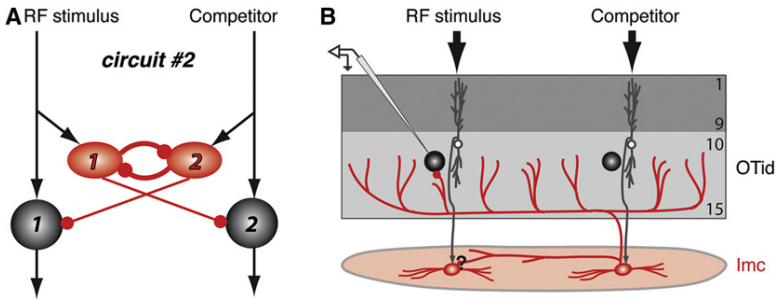

Figure 4. Model Circuit 2: Reciprocal Inhibition among Feedforward Lateral Inhibitory Elements

(A) Conventions as in Figure 1B. Compared to model circuit 1, this circuit has one modification: reciprocal inhibition among the feedforward lateral inhibitory elements.

(B) Conventions as in Figure 1A. Schematic of key elements of the midbrain network showing Imc axon branches that, in addition to projecting broadly back to the OT (Figure 1A), terminate within the Imc as well (Wang et al., 2004). Whether these terminals form functional inhibitory synapses onto other Imc neurons is yet to be tested.

See also Figure S3.

(reciprocal inhibitory connections; Figure 4A). Indeed, structural support for such a circuit motif in the Imc has been found in an anatomical study (Wang et al., 2004). The study showed that in addition to projecting to the OTid, Imc axonal branches also terminate within the Imc itself (Figure 4B). Such reciprocal connections will cause the inhibitory units representing each location to inhibit the inhibitory units representing all other locations. As a result, the activity of each inhibitory unit should depend on the strength of its excitatory drive relative to the excitatory drive to other inhibitory units.

To model the reciprocal connectivity, we first modeled each inhibitory unit as being affected by a combination of input and output divisive inhibition (along with an implicit subtractive component; Equation 6). This formulation was general, because it allowed for the inhibition onto inhibitory units to be any arbitrary combination of the commonly observed forms of inhibition in the literature.

$$I(t) = \left(\frac{1}{i_{out}(t)+1}\right) \cdot \left(\frac{m}{i_{in}(t)+1} + h\left(\frac{I^k}{I^k + s_{50}^k + (i_{in}(t))^k}\right)\right) \quad (6)$$

Here, *I(t)* is the inhibitory activity at computational time-step t. $i_{in}(t)$ and $i_{out}(t)$ were the input and output divisive factors at time-step t, modeled as being proportional to the activity of the inhibitory units at the previous time step (compare to Equation 4):

$$i_{in}(t) = r_{in} \cdot I(t-1), i_{out}(t) = r_{out} \cdot I(t-1) \quad (7)$$

r_{in} and r_{out} are proportionality constants. In this formulation, transmission and synaptic delays were assumed to be equal to one computational time step, for simplicity. These equations were applied iteratively until there was no further change in the inhibitory activity, i.e., *I(t) = I(t+1)*. The resulting steady-state activity of the inhibitory units was referred to as I_{ss}. Consequently, at steady state, the input and output divisive factors in Equation 7 reduce to

$$i_{in} = r_{in} \cdot I_{ss}, i_{out} = r_{out} \cdot I_{ss} \quad (8)$$

The single-stimulus-response functions of the inhibitory and excitatory units were unchanged from before.

Before exploring the effect of reciprocal inhibition on output unit activity, we first analyzed its effect on the steady-state inhibitory activity. We plotted I_{ss} for inhibitory unit 2 during a CRP measurement protocol, with an RF stimulus of strength 8°/s (Figures S3A and S3B). Compared to the inhibitory activity obtained with circuit 1 (Figure S2E), the steady-state inhibitory activity obtained with circuit 2 (Figure S3B) displayed two key differences. First, the rate of increase in inhibitory activity with increasing competitor strength was steeper in the presence of reciprocal inhibition (Figure S3B, solid magenta versus dashed magenta lines). This increase in steepness reflected, as expected, an iterative amplification of the difference in activity between the two inhibitory units, due to the inhibitory feedback motif. Second, when another CRP was obtained with a different RF stimulus (14°/s), the steady-state inhibitory activity of inhibitory unit 2 was conspicuously shifted to the right (Figure S3B, solid blue versus solid magenta), in contrast to the results from the feedforward circuit (Figure S2E). This rightward shift in the steady-state inhibitory activity predicted that, following a change in the strength of the RF stimulus, output unit CRPs would also shift adaptively. We tested this prediction below. For subsequent simulations, we chose the reciprocal-inhibitory parameter values as follows: r_{in} = 0.84 (which yielded the maximum rightward shift of the inhibitory activity; Figure S3C) and r_{out} = 0.01 (Figure S3D).

Results from Model Circuit 2

We asked whether a circuit with reciprocal inhibition of feedforward lateral inhibition could produce the two response signatures critical for categorization in the OTid.

Reciprocal Inhibition of Feedforward Lateral Inhibition Can Produce Switch-like CRPs

To test whether this circuit model can produce switch-like CRPs at the output (OTid) units, we simulated output unit CRPs and, as before (Figure 3B), plotted their transition ranges as a function of each of the parameters of the inhibitory-response function (Figure 5B). For these plots, the values of d_{in} and d_{out} and the values of the fixed inhibitory parameters were chosen to be the same as those used previously in testing circuit 1 (Figure 3B).

We found that large enough values of the saturation parameter *k* and small enough values of the half-maximum response loom speed (S_{50}) yielded switch-like CRPs (Figure 5B). An example of a switch-like CRP, obtained with the same values of the inhibitory parameters used for circuit 1 (Figure 3C), is shown in Figure 5C. As expected by the steeper inhibitory-response function (Figure S3B, solid versus dashed magenta), this CRP at the output unit is also steeper (compare with Figure 3C).

Reciprocal Inhibition of Feedforward Lateral Inhibition Can Produce Adaptive Shifts of CRPs

Next, we tested whether this circuit can produce adaptive shifts in the CRP switch value. As before, we asked whether any combination of input and output divisive inhibition (d_{in} and d_{out},

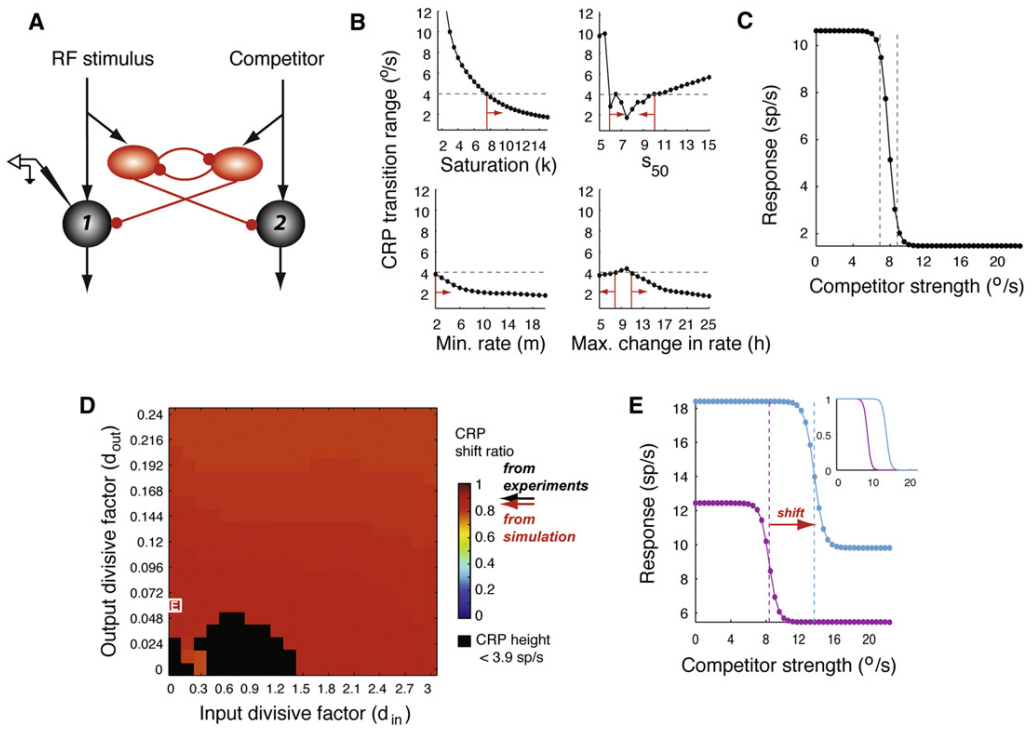

Figure 5. Reciprocal Inhibition among Feedforward Lateral Inhibitory Elements, Circuit 2, Can Produce Switch-like CRPs and Adaptive Shifts in CRP Switch Value

(A) Schematic of circuit 2. Recording icon indicates the unit for which responses are shown in (B) and (C).

(B) Effect of varying the parameters of the inhibitory-response function on the CRP transition range of output unit 1. Red line and arrow indicate the range of values of a parameter over which CRPs are switch like (transition ranges $\leq 4°$/s). The value of the indicated parameter was varied systematically while the other parameters were held at the following fixed values: $k = 10$, $S_{50} = 8$, $m = 5$, $c = 15$, $d_{in} = 1$, and $d_{out} = 0.05$; same values as in Figure 3B. The reciprocal inhibition factors r_{in} and r_{out} were chosen to be 0.84 and 0.01, respectively (see Results; Figures S3C and S3D).

(C) The switch-like CRP produced after choosing the values of the parameters of the inhibitory-response function to be $k = 10$, $S_{50} = 8$, $m = 5$, $c = 15$, $d_{in} = 1$, and $d_{out} = 0.05$; same as in Figure 3C.

(D) CRP shift ratio (shift in CRP switch value / change in the strength of the RF stimulus) as a function of the input and output divisive normalization factors (d_{in} and d_{out}; ranges of d_{in} and d_{out} same as in Figure 3D). Reciprocal inhibition parameters r_{in} and r_{out} were set at 0.84 and 0.01, respectively (Results). All other parameter values were same as in Figure 3D. The change in the RF stimulus strength was 6°/s. The black-shaded values indicate (d_{in}, d_{out}) pairs that yielded CRPs for which at least one of them had a maximum change in response less than the threshold of 3.9°/s (Experimental Procedures) or for which one of the CRPs was not switch like (transition range > 4°/s). Largest value of CRP shift ratio = 0.88, obtained for the (d_{in}, d_{out}) pair = (0, 0.06), indicated by the boxed letter E. The resulting CRPs are shown in (E). Note, however, that a large range of nonzero d_{in} and d_{out} values yielded CRP shift ratios very close to the maximal value (Figure S4A).

(E) The two CRPs corresponding to the (d_{in}, d_{out}) pair that yielded the largest CRP shift ratio ($d_{in} = 0$, $d_{out} = 0.06$). Inset represents normalized CRPs.

See also Figure S4.

respectively; Equations 2 and 3) could produce a shift in the CRP switch value with a 6°/s increase in the RF stimulus strength. The strength of reciprocal inhibition was unchanged from before ($r_{in} = 0.84$ and $r_{out} = 0.01$).

A plot of model CRP shift ratios (ratio of switch-value shift to change in RF stimulus strength) as a function of d_{in} and d_{out} shows that a large set of (d_{in}, d_{out}) values successfully produced adaptive shifts in the switch value (shift ratio near 1; Figure 5D and Figure S4A). The ranges of d_{in} and d_{out} tested were the same as those used for testing the feedforward circuit (Figure 3D). The largest CRP shift ratio (for this particular set of r_{in} and r_{out} values) was 0.88, nearly identical to the average value of shift ratios observed experimentally (0.90 ± 0.16; Mysore et al., 2011). The two CRPs that yielded this shift ratio are shown in Figure 5E. In addition to displaying a rightward shift, the CRP computed with the stronger RF stimulus (Figure 5E, blue curve) was scaled upwards with respect to the CRP that was computed with the weaker RF stimulus (Figure 5E, magenta curve), consistent with experimental results (Figure 2E; Mysore et al., 2011). However, when divisive inhibition was exceptionally strong, the scaling of the responses to the losing RF stimulus was eliminated, resulting in winner-take-all responses.

The strengths of reciprocal inhibition and the values of the parameters of the inhibitory-response functions chosen to demonstrate these rightward shifts were not special. Wide ranges of values for these parameters produced adaptive shifts in the CRP switch value (Figure S4).

Thus, reciprocal inhibition between feedforward lateral inhibitory units can produce switch-like CRPs and adaptive shifts in the switch value in response to changes in RF stimulus strength,

Table 1. Comparison of the Properties of Target-with-Competitor versus Target-Alone Response Profiles

Property of Response Profile	Measured in Feedforward Lateral Inhibition (Circuit 1) Figure 2C	Measured in Circuit with Reciprocal Inhibition of Feedforward Lateral Inhibition (Circuit 2) Figures 6A–6G
Dynamic range	Wider than (or) equal to	Wider than (or) equal to (or) narrower than (Figures 6A, 6D, and 6F)
Suppression of responses to the weakest versus the strongest RF stimulus	Equal to (or) less than	Equal to (or) less than (or) more than (Figures 6C and 6E)
Half-maximum response strength: relation to half-maximum response strength of TaRP	Right-shifted (or) unchanged	Right-shifted (or) unchanged
Half-maximum response strength: relation to competitor strength	Proportional (or) none	Equal, on average (Figure 6G)

thereby creating an explicit and flexible categorical representation of stimuli based on relative stimulus strength.

Model Predictions

Thus far, we have demonstrated that model circuit 2, involving the reciprocal inhibition of lateral inhibition motif, successfully accounts for experimentally measured CRP properties. To further evaluate the validity of this circuit, we used it to predict output unit activity in a different two-stimulus paradigm, one that had not been previously tested experimentally. In this paradigm, the responses to a receptive-field stimulus of increasing strength were obtained both without a competitor and with a competitor of fixed strength. The resulting profiles of output unit activity are called, respectively, the "target-alone response profile" and the "target-with-competitor response profile." Comparing these profiles allowed us to assess the effect of a fixed competitor strength on the classic, strength-response profile.

We show next that model circuit 2 predicts a wide range of shapes for target-with-competitor response profiles, the bulk of which are not predicted by model circuit 1. We also demonstrate with additional experimental results that neuronal responses to this two-stimulus paradigm are fully in line with the predictions of model circuit 2, but not model circuit 1.

The feedforward lateral inhibitory circuit (circuit 1, Figure 1B) produced target-with-competitor response profiles that reflected, essentially, various combinations of purely input divisive (Figure 2C, left) and purely output divisive (Figure 2C, right) influences caused by the competitor stimulus. The full range of effects is summarized in Table 1 (middle column) and is typical of structures that process sensory information (Cavanaugh et al., 2002; Olsen et al., 2010; Williford and Maunsell, 2006).

Addition of the reciprocal-inhibition motif to the feedforward lateral inhibitory circuit (circuit 2, Figure 4B) yielded not only target-with-competitor response profiles that were similar to those described above (Figures 6A and 6B), but also, importantly, profiles that were qualitatively distinctive in each of three respects (Figures 6C–6E, 6F, and 6G), as summarized in Table 1 (last column). These kinds of effects are not typically observed in structures that process sensory features. Thus, the two circuit models make predictions that are qualitatively different.

Testing Model Predictions

We tested these strong predictions of the models experimentally in the barn owl OTid. For each OTid neuron, we measured target-alone response profiles by varying the strength (loom speed) of a stimulus presented at the center of the RF (n = 71 neurons). Randomly interleaved with these were the target-with-competitor response profiles, measured with a second simultaneously presented competitor stimulus, located far outside the RF (30° away). The responses were fit with sigmoidal functions, and various parameters of the fit were estimated and compared to predictions.

The range of effects on loom speed-response profiles observed in the OTid that were due to the presence of a competitor stimulus matched those predicted by model circuit 2 and exceeded those predicted by model circuit 1. In addition to target-with-competitor response profiles that reflected pure feedforward input or output division (Figures 6H and 6I compared with Figures 6A and 6B), we found target-with-competitor response profiles that exhibited smaller dynamic ranges (Figures 6J and 6K), more suppression of the responses to the weakest than the strongest RF stimulus (Figures 6J and 6L), as well as right-shifted (Figures 6H and 6J–6L) or unshifted (Figure 6I) half-maximum response strengths. These representative results were confirmed by population analyses (Figures 6M–6O2).

The correspondence between the predictions made by model circuit 2 and the experimental results supports the validity of the reciprocal inhibition of feedforward lateral inhibition model.

Advantages of the Reciprocal Inhibition of Feedforward Lateral Inhibition Circuit over Alternative Circuit Models

Reciprocal inhibition among feedforward lateral inhibitory units is only one of many circuit architectures for producing competitive inhibition that adapts to the relative strengths of drive to competing stimulus channels. Alternative circuits that accomplish the same goal include feedback inhibition among output units (Figure 7A, circuit 3), feedback inhibition from output units to input units (Figure 7C), and each of these circuits with an additional recurrent excitatory loop (Figures 7B and 7D, respectively). However, reciprocal inhibition of feedforward lateral inhibition accomplishes the computational goal with structural efficiency: by interconnecting the inhibitory units themselves, the inhibitory drive from each competing channel is modulated directly by the inhibitory drives from all other channels. With this motif, the feedback loop involves only the inhibitory units and the two synapses that connect them. In contrast, all other feedback architectures involve additional units and synapses in the feedback loop.

We studied the consequences of structural complexity of the feedback motif on the ability of the model to compute steady-state responses to competing stimuli rapidly and reliably. We compared the performance of the reciprocal inhibition of feedforward lateral inhibition motif (Figure 4, circuit 2) with that of the next most structurally simple motif: feedback lateral inhibition by output units (Figure 7A, circuit 3). The parameter values for the circuit 2 model were chosen to be the same as those in Figure 5E. The parameter values for the circuit 3 model were chosen such that the circuit yielded output unit responses at steady state that were nearly identical to those from the circuit 2 model (Figures S5A–S5D). The quality of the match between the responses of the two circuits was particularly sensitive to the values of the parameters for circuit 3, with the best match occurring over a narrow range of values (Figures S5E–S5J).

We measured calculation speed as the settling time, defined as the first time step after which responses did not change any further (Experimental Procedures). The time courses of the responses from the two models, calculated for an RF stimulus of strength of 9°/s and a competitor strength of 8°/s (relative strength = 1°/s), demonstrated that circuit 2 settled faster than circuit 3 (Figure 7E). This finding held true for all relative stimulus strength values (Figure 7F). Both models exhibited longer settling times as the relative strength between the competing stimuli decreased, consistent with the experimental observation that difficult discriminations take longer to resolve (Gold and Shadlen, 2007).

We assessed the reliability of the calculation as the consistency of the steady-state response. Gaussian noise was introduced into the calculation of the response for each unit at each time step. Consistency was quantified by calculating the Fano factor (Experimental Procedures), a metric that is inversely related to response consistency. The distribution of Fano factors at steady state was estimated using Monte Carlo analyses (Experimental Procedures).

Comparison of the Fano factors from the two models for an RF stimulus of strength of 9°/s and a competitor strength of 8°/s (relative strength = 1°/s) showed that circuit 2 produced less variability (smaller Fano factor) than circuit 3 (Figure 7G; average Fano factors were 0.71 ± 0.01 and 0.78 ± 0.01, respectively; $p < 10^{-4}$, rank-sum test). Circuit 2 exhibited superior reliability for all values of the RF stimulus from 1°/s to 9°/s (competitor = 8°/s), with the reduction in Fano factor being substantial (approximately 75%) when the RF stimulus was weaker or as strong as the competitor (Figure 7H). When the RF stimulus was substantially stronger than the competitor (RF stimulus strengths = 11°/s–16°/s), the Fano factors yielded by circuit 2 were slightly greater than those yielded by circuit 3 (Figure 7H). Considered together, these effects show that for all values of relative stimulus strength, the discriminability between the responses to the stronger (winning) stimulus and the weaker (losing) stimulus is substantially greater for the circuit 2 model that contained the inhibition of inhibition motif.

Thus, the structural simplicity of the reciprocal inhibition of feedforward lateral inhibition motif enabled both faster and more reliable categorization of competing stimuli than the next most structurally simple implementation of this competitive rule.

DISCUSSION

Although flexible categorization has been studied extensively in systems and cognitive neuroscience, how neural circuits might implement it has been unclear. Our goal was to provide an intuitive, circuit level account of the key computations involved in creating an explicit and flexible categorization of stimuli while being agnostic to their biophysical implementation. Through a first principles approach, we showed that although classical feedforward lateral inhibition, implemented with sufficiently steep inhibitory stimulus-response functions, can successfully produce categorical responses, it cannot adjust the category boundary flexibly in response to changes in the absolute strengths of competing stimuli. In contrast, relative strength-dependent lateral inhibition (feedback inhibition) achieves both explicit and flexible categorization. Although many different circuits can implement relative strength-dependent inhibition, reciprocal inhibition among the feedforward lateral inhibitory units is structurally the simplest, involving the fewest possible units and synapses within the feedback loop, and it categorizes stimuli faster and more reliably than the next simplest circuit. The superior performance of this motif suggests that it may occur in networks that are engaged in flexible categorization, identification, or decision making, particularly when speed or reliability is important.

Reciprocal inhibition of inhibitory elements is a circuit motif that has been observed in several other brain areas, such as the thalamic reticular nucleus (Deleuze and Huguenard, 2006), the neocortex (Pangratz-Fuehrer and Hestrin, 2011), and the hippocampus (Picardo et al., 2011). However, a clear function for this circuit motif has not been ascribed. Our analysis indicates that the primary power of this circuit motif is in both enhancing and providing flexibility to the comparison of information across channels.

Normalization Models of Sensory Processing

The feedforward lateral inhibition motif, which served as the core of the model in this study, has been employed widely in models of sensory information processing and attentional modulation of sensory representations. One of these models was of olfactory processing in the fly antennal lobe (Olsen et al., 2010). In that study, the effect of increasing the strength of a competing stimulus on the representation of an RF stimulus (which we call a CRP) was tested with RF stimuli of different strengths. Consistent with our results, they report no adaptive shifts in CRPs with changing RF stimulus strengths from this feedforward lateral inhibitory circuit.

In one model of information processing in the primate visual cortex (V1), nonlinear properties of response normalization, consistent with input divisive normalization, were accounted for with feedback inhibition (Carandini et al., 1997). Our study and others (Olsen et al., 2010; Pouille et al., 2009) have demonstrated, however, that a feedforward circuit is sufficient to achieve input divisive normalization. The necessity for feedback inhibition in that study was not explored. Our results, and those from a recent model of V1 (Ayaz and Chance, 2009), indicate that feedback inhibition enhances the nonlinearity of competitive-response profiles. In addition, our results indicate that feedback inhibition is required for adaptive shifts of CRPs of the kind observed in V1

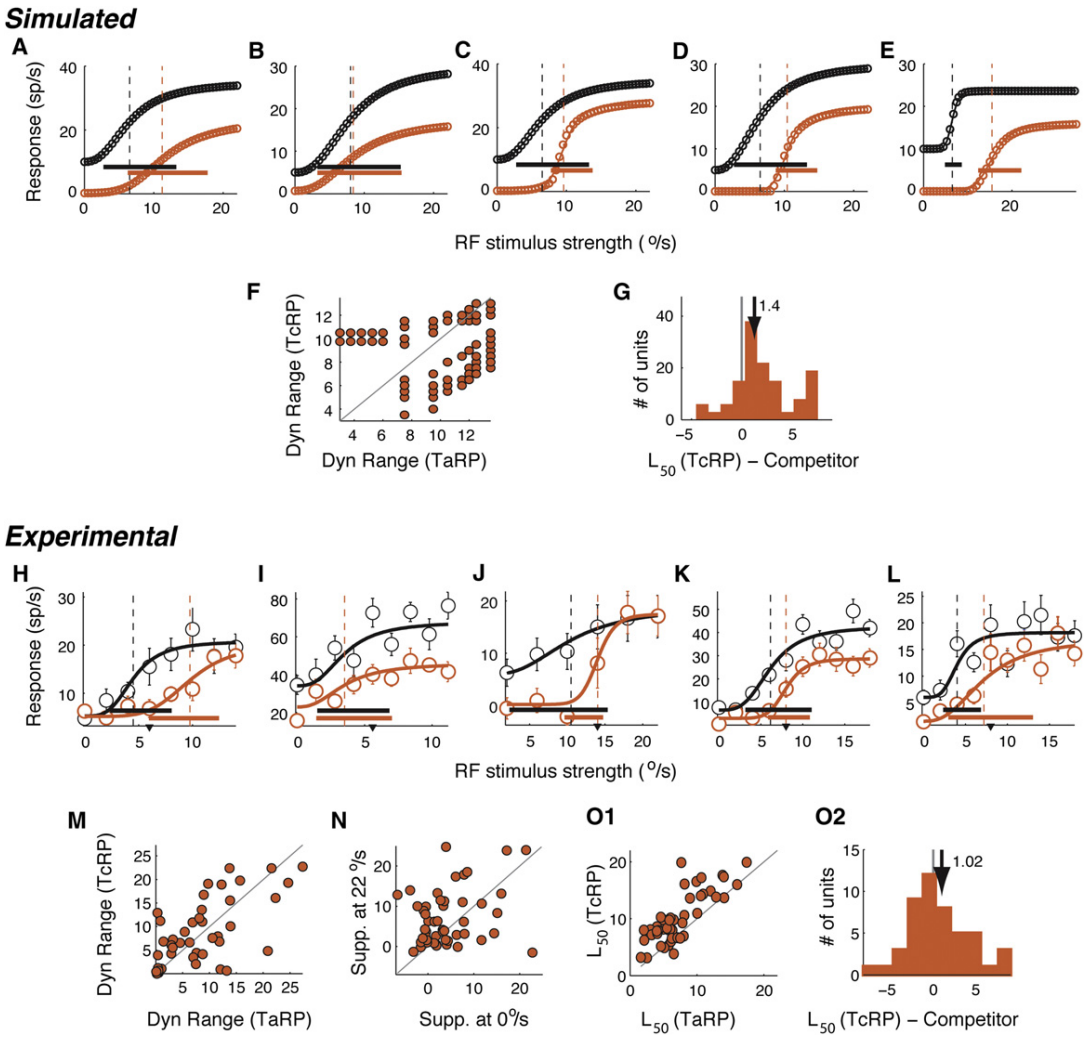

Figure 6. Comparison of Model Predictions with Experimental Data from the Owl OTid

(A–G) Simulated data calculated for output unit 1 in circuit 2 (Figure 4A).

(A–E) Simulated loom speed-response functions obtained from model circuit 2 using different sets of parameter values to illustrate the range of effects of a fixed-strength competing stimulus, described in the Results. The values of the parameters used to generate these curves are listed in Table S1. Black represents target-alone response profiles, orange shows target-with-competitor response profiles, dashed vertical lines indicate the location of the half-maximum response speeds, and solid horizontal lines indicate the dynamic ranges. Error bars indicate SEM.

(F) Scatterplot of dynamic ranges. Diagonal line represents line of equality.

(G) Distribution of the difference between the half-maximum response speed (L_{50}) of the target-with-competitor response profile and the strength of the competitor.

(F and G) 135 pairs of target-alone response profile and target-with-competitor response profile were generated by varying the half-maximum response speed (S_{50}) of the output units systematically over nine values (from 4°/s through 12°/s) and by varying the half-maximum response speed of the inhibitory units (from 7°/s through 9°/s) while holding all other parameter values constant. The strength of the competitor was always 8°/s.

(H–O2) Experimental results based on measurements of loom speed-response functions from 51/71 OTid units for which (1) both response profiles (target-alone response profile and target-with-competitor response profile) were correlated with the strength of RF stimulus, (2) they were well fit by sigmoids ($r^2 > 0.8$), and (3) there was an effect of the competitor (Experimental Procedures). Median strength of competitor = 8°/s.

(H–L) Loom speed-response functions measured without (black) and with (orange) a competitor stimulus located 30° to the side of the RF. The strength of the competitor in each case is indicated by the position of the black triangle on the x axis. Dashed vertical lines indicate the location of the half-maximum response speeds (L_{50}). Solid horizontal lines indicate the dynamic ranges.

(M) Scatterplot of dynamic ranges of target-with-competitor response profiles (TcRPs) versus those of target-alone response profiles (TaRPs), showing several neurons that had narrower dynamic ranges in the presence of the competitor (Experimental Procedures). Diagonal line represents line of equality. Similar to model predictions in (F).

(N) Scatterplot of the amount of suppression (spikes/s) of responses to the strongest RF stimulus (22°/s) versus suppression to the weakest RF stimulus (0°/s), showing several neurons with greater suppression of the responses to the weakest RF stimulus. Diagonal line represents line of equality.

(Carandini et al., 1997). In sensory processing, then, feedback lateral inhibition causes normalization that adjusts adaptively according to relative stimulus strengths, and reciprocal inhibition of feedforward lateral inhibition could be an efficient circuit motif to implement such a flexible normalization rule.

Other models of sensory normalization, particularly those simulating interactions of stimuli within the RF (like crossorientation suppression in V1 or biased stimulus competition for attention), typically invoke mechanisms that are distinct from those that affect responses outside of the RF explored in this study (Busse et al., 2009; Carandini et al., 2002; Freeman et al., 2002; Lee and Maunsell, 2009; Ohshiro et al., 2011; Reynolds et al., 1999; Reynolds and Heeger, 2009).

Comparison with Models of Selection for Action and Attention

Different kinds of models have been proposed to explain the major steps in stimulus selection for action or attention (Cisek and Kalaska, 2010; Itti and Koch, 2001; Lee et al., 1999), with one step being a winner-take-all operation (Edwards, 1991; Hahnloser et al., 1999; Koch and Ullman, 1985), which we have shown to be a special case of flexible categorization. However, these models were strictly computational, with no explicit correspondence between component computations and neural circuitry.

The patterns of connections within the midbrain network facilitate the inference of component computations from neural structure. The striking anatomy of the GABAergic Imc circuit (Figure 4B) has inspired the proposal that it participates in a winner-take-all selection of the highest priority stimulus (Marín et al., 2007; Sereno and Ulinski, 1987). A recent model of this network (Lai et al., 2011) invoked connections between the optic tectum, the Imc, and a cholinergic nucleus in the isthmic complex (Asadollahi et al., 2010) to attempt to explain winner-take-all responses. Although the circuit model used was a variation of the model in Figure 7B, one of the circuits that can produce explicit and flexible categorization (Figures S5A–S6D; Koch and Ullman, 1985), their particular choice of parameter values did not yield flexible categorization.

Our study suggests that the Imc circuit can, by itself, mediate categorization in the midbrain network. We propose a simpler and faster circuit motif for implementing flexible categorization and, possibly, winner-take-all decisions: reciprocal inhibition of feedforward lateral inhibition within the Imc. Anatomical support for such a motif has been found in a study of the projection patterns of Imc neurons (Figure 4B; Wang et al., 2004). Future experiments will be needed to determine the contribution of the Imc to categorization in controlling gaze and attention.

Generality of the Reciprocal Inhibition of Feedforward Lateral Inhibition Motif

The computations explored in this study that account for explicit and flexible categorization of relative stimulus strengths in the midbrain network may generalize to other examples of categorical decisions and, therefore, to other brain areas (Wang, 2008). Classification of direction of stimulus motion with respect to a flexible reference (Freedman and Assad, 2006), of speed of stimulus motion with respect to a flexible reference (Ferrera et al., 2009), of odor based on relative odor strengths in a mixture (Niessing and Friedrich, 2010), and of tactile stimulus frequency relative to a prior sample frequency (Machens et al., 2005) can each be thought of as decisions based on such categorization. Indeed, the model that was proposed to account for neural responses in the monkey prefrontal cortex during the discrimination of tactile stimulus frequency relative to a prior sample frequency employed feedback inhibition (Machens et al., 2005). In this task, the decision of whether the test frequency was higher or lower than the sample frequency can be thought of as a form of flexible categorization, in which the comparison of stimulus representations occurs over time rather than space. Like other models of decision, the model that was proposed was purely computational and without neural correlates, and the specific computational contributions of the different circuit elements to the decision were not explored.

Recently, parallels between such potentially abstract decision-making processes and competitive stimulus selection have been recognized (Cisek and Kalaska, 2010; Freedman and Assad, 2011). We propose that reciprocal inhibition of feedforward lateral inhibition, which works in various brain areas, could serve as a highly efficient motif for flexible categorization for decisions, as well as for flexible normalization.

EXPERIMENTAL PROCEDURES

Computational Modeling

Data Analysis

The transition range of a CRP was defined as the range of competitor strengths over which responses dropped from 90% to 10% of the total range of responses. Switch-like CRPs were defined as those for which the CRP transition range was $\leq 4°$/s (Mysore et al., 2011).

The switch value of a switch-like CRP was defined as the strength of the competitor stimulus at which responses to the paired stimuli changed from high to low values. It was estimated as the competitor strength that yielded the half-maximum response.

CRP height was measured as the difference between the maximum and minimum responses over the standard range of competitor loom speeds (0°/s–22°/s). For experimentally measured CRPs, we estimated maximum and minimum responses from the best sigmoidal fit to the data. Experimental results (Mysore et al., 2011) indicate that only ~70% of CRPs measured in the OTid are significantly correlated with the strength of the competitor stimulus ("correlated CRPs"); for the remaining CRPs, the maximum change in response with competitor strength ("CRP height," Experimental Procedures) is not large enough to yield a significant correlation. The smallest value of CRP height for correlated CRPs, estimated as the fifth percentile value of the distribution of heights for such CRPs, was 3.9 sp/s (n = 107). To translate this constraint to our model, we considered simulated CRPs with heights smaller than the 3.9 sp/s to be not correlated, and we excluded them from subsequent analysis.

(O1) Scatterplot of half-maximum response speeds (L_{50}) of TcRPs versus those of TaRPs, showing that TcRPs are typically right shifted with respect to TaRPs. Diagonal line represents line of equality.

(O2) Plot of the difference between the half-maximum response speed (L_{50}) of the TcRP and the strength of the competitor, showing that the distribution is centered around 0 ($p > 0.05$, t test against 0). Similar to model predictions in (G).

See also Table S1.

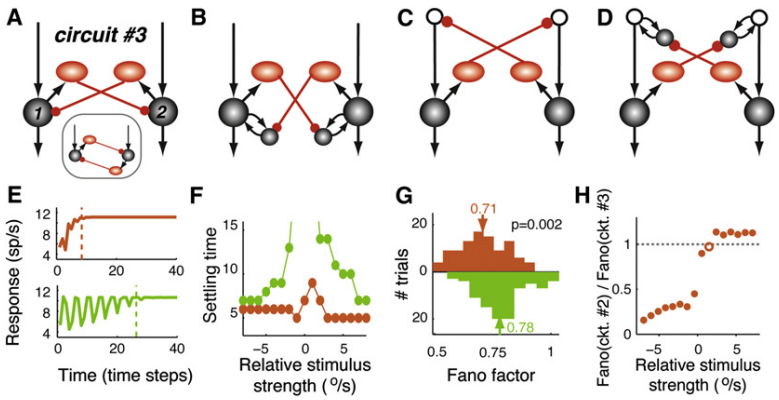

Figure 7. Comparison of the Performance of Alternative Circuit Implementations of Feedback Lateral Inhibition

(A–D) Alternatives to model circuit 2 (Figure 4) that also implement adaptive, competitive lateral inhibition.

(A) Feedback lateral inhibition by output units; inset represents equivalent circuit.

(B) Same as (A), but with additional recurrent excitatory loops to output units.

(C) Feedback lateral inhibition to input units.

(D) Same as (C), but with additional recurrent excitatory loops to input units.

(E and F) Comparison of settling times for circuit 2 (orange) and the next-simplest circuit, circuit 3 (green), shown in (A).

(E) Examples of time courses of responses to an RF stimulus strength of 9°/s and a competitor stimulus strength of 8°/s. Top: circuit 2. Bottom: circuit 3. Dashed lines represent settling time (Experimental Procedures).

(F) Settling time as a function of relative stimulus strength (RF stimulus strength − competitor strength). Competitor strength was held constant at 8°/s. Orange represents circuit 2, and green indicates circuit 3.

(G and H) Comparison of the reliability of the two circuits.

(G) Monte Carlo simulation was used to generate 100 estimates of the Fano factor (a metric that is inversely related to response consistency; Experimental Procedures) for the steady-state response (at t = 100 time steps) with an RF stimulus strength of 9°/s and a competitor strength of 8°/s (Experimental Procedures). Orange represents circuit 2, and green indicates circuit 3.

(H) Ratio of the mean Fano factor yielded by circuit 2 to that yielded by circuit 3, as a function of the relative stimulus strength (RF stimulus strength − competitor strength). Competitor strength was held constant at 8°/s. Filled circles indicate $p < 0.05$ (pairwise rank-sum test between Fano factor distributions at each value of relative stimulus strength followed by Holm-Bonferroni correction for multiple comparisons); open circle indicates $p > 0.05$.

(E)–(H)For the simulations, the parameter values of circuit 2 were the same as in Figure 5E. The parameters for circuit 3 were chosen to be optimal (minimum model error; Figure S5 and Experimental Procedures): $d_{in} = 1.1$, $d_{out} = 0.005$, $m = 1$, $h = 21$, $S_{50} = 9$, and $k = 5$.

See also Figure S5.

The dynamic range of either a target-alone response profile or a target-with-competitor response profile was defined, analogous to the CRP transition range, as the range of RF stimulus loom speeds over which responses increased from 10% to 90% of the total range of responses. Both the transition and dynamic ranges are directly related to the maximum (normalized) slope of the responses: smaller dynamic range <=> higher maximum (normalized) slope.

For circuits involving inhibitory feedback (Figures 4A and 7A) in which steady-state responses were iteratively computed, the speed at which steady state was achieved was quantified using response settling time. This was defined as the first iteration time step at which the response did not change any further (<5% change thereafter).

To estimate the reliability of the responses produced by these circuits, we introduced Gaussian noise at each computation of a unit's response using its input-output function. The standard deviation of the noise of the response was assumed to be proportional to its mean (SD = mean/5). Monte Carlo simulation was used to obtain multiple (n = 100) estimates of the steady-state response.

Response variability was estimated using the Fano factor, defined as the ratio of the variance of the responses to the mean of the responses to a given stimulus strength. This procedure was repeated 100 times to estimate the distribution of the Fano factor.

The model error quantified the mismatch in the responses of output unit 1 in circuit 3 with respect to the responses of output unit 1 in circuit 2. It was computed by simulating the responses with both circuits to four stimulus protocols: target-alone response profile, target-with-competitor response profile, CRP1, and CRP2. The absolute values of the differences in responses between the two circuits for all four protocols were added up to yield the model error.

Neurophysiology

Experimental Protocol

Experiments to test the model predictions were performed following protocols that have been described previously (Mysore et al., 2010, 2011), and key aspects are listed in the Supplemental Experimental Procedures. Briefly, epoxy-coated tungsten microelectrodes (FHC, 250 μm, 1–5 MW at 1 kHz) were used to record single units and multiunits extracellularly in seven barn owls that typically were tranquilized with a mixture of nitrous oxide and oxygen. Multiunit spike waveforms were sorted offline into putative single units. All recordings were made in layers 11–13 of the optic tectum (OTid). Visual looming stimuli were presented on a tangent screen in front of the owl.

SUPPLEMENTAL INFORMATION

Supplemental Information includes five figures, one table, and Supplemental Experimental Procedures and can be found with this article online at doi:10.1016/j.neuron.2011.10.037.

ACKNOWLEDGMENTS

This work was supported by funding from the National Institutes of Health (9R01 EY019179-30, to E.I.K.). We thank Daniel Kimmel, Valerio Mante, and Alireza Soltani for critically reading the manuscript and for discussions. S.P.M. and E.I.K. designed the research and wrote the manuscript. S.P.M. performed the simulations, experiments, and analyses.

Accepted: October 14, 2011
Published: January 11, 2012

REFERENCES

Allman, J., Miezin, F., and McGuinness, E. (1985). Stimulus specific responses from beyond the classical receptive field: neurophysiological mechanisms for local-global comparisons in visual neurons. Annu. Rev. Neurosci. *8*, 407–430.

Asadollahi, A., Mysore, S.P., and Knudsen, E.I. (2010). Stimulus-driven competition in a cholinergic midbrain nucleus. Nat. Neurosci. *13*, 889–895.

Ayaz, A., and Chance, F.S. (2009). Gain modulation of neuronal responses by subtractive and divisive mechanisms of inhibition. J. Neurophysiol. *101*, 958–968.

Blakemore, C., and Tobin, E.A. (1972). Lateral inhibition between orientation detectors in the cat's visual cortex. Exp. Brain Res. *15*, 439–440.

Bolzon, D.M., Nordström, K., and O'Carroll, D.C. (2009). Local and large-range inhibition in feature detection. J. Neurosci. *29*, 14143–14150.

Busse, L., Wade, A.R., and Carandini, M. (2009). Representation of concurrent stimuli by population activity in visual cortex. Neuron *64*, 931–942.

Carandini, M., Heeger, D.J., and Movshon, J.A. (1997). Linearity and normalization in simple cells of the macaque primary visual cortex. J. Neurosci. *17*, 8621–8644.

Carandini, M., Heeger, D.J., and Senn, W. (2002). A synaptic explanation of suppression in visual cortex. J. Neurosci. *22*, 10053–10065.

Cavanaugh, J., and Wurtz, R.H. (2004). Subcortical modulation of attention counters change blindness. J. Neurosci. *24*, 11236–11243.

Cavanaugh, J.R., Bair, W., and Movshon, J.A. (2002). Nature and interaction of signals from the receptive field center and surround in macaque V1 neurons. J. Neurophysiol. *88*, 2530–2546.

Cisek, P., and Kalaska, J.F. (2010). Neural mechanisms for interacting with a world full of action choices. Annu. Rev. Neurosci. *33*, 269–298.

Deleuze, C., and Huguenard, J.R. (2006). Distinct electrical and chemical connectivity maps in the thalamic reticular nucleus: potential roles in synchronization and sensation. J. Neurosci. *26*, 8633–8645.

Edwards, D.H. (1991). Mutual inhibition among neural command systems as a possible mechanism for behavioral choice in crayfish. J. Neurosci. *11*, 1210–1223.

Ferrera, V.P., Yanike, M., and Cassanello, C. (2009). Frontal eye field neurons signal changes in decision criteria. Nat. Neurosci. *12*, 1458–1462.

Freedman, D.J., and Assad, J.A. (2006). Experience-dependent representation of visual categories in parietal cortex. Nature *443*, 85–88.

Freedman, D.J., and Assad, J.A. (2011). A proposed common neural mechanism for categorization and perceptual decisions. Nat. Neurosci. *14*, 143–146.

Freedman, D.J., Riesenhuber, M., Poggio, T., and Miller, E.K. (2001). Categorical representation of visual stimuli in the primate prefrontal cortex. Science *291*, 312–316.

Freeman, T.C., Durand, S., Kiper, D.C., and Carandini, M. (2002). Suppression without inhibition in visual cortex. Neuron *35*, 759–771.

Gold, J.I., and Shadlen, M.N. (2007). The neural basis of decision making. Annu. Rev. Neurosci. *30*, 535–574.

Gollisch, T., and Meister, M. (2010). Eye smarter than scientists believed: neural computations in circuits of the retina. Neuron *65*, 150–164.

Hahnloser, R., Douglas, R.J., Mahowald, M., and Hepp, K. (1999). Feedback interactions between neuronal pointers and maps for attentional processing. Nat. Neurosci. *2*, 746–752.

Hartline, H.K., Wagner, H.G., and Ratliff, F. (1956). Inhibition in the eye of Limulus. J. Gen. Physiol. *39*, 651–673.

Itti, L., and Koch, C. (2001). Computational modelling of visual attention. Nat. Rev. Neurosci. *2*, 194–203.

Knudsen, E.I. (2011). Control from below: the role of a midbrain network in spatial attention. Eur. J. Neurosci. *33*, 1961–1972.

Koch, C., and Ullman, S. (1985). Shifts in selective visual attention: towards the underlying neural circuitry. Hum. Neurobiol. *4*, 219–227.

Kuffler, S.W. (1953). Discharge patterns and functional organization of mammalian retina. J. Neurophysiol. *16*, 37–68.

Lai, D., Brandt, S.F., Luksch, H., and Wessel, R. (2011). Recurrent antitopographic inhibition mediates competitive stimulus selection in an attention network. J. Neurophysiol. *105*, 793–805.

Lee, J., and Maunsell, J.H. (2009). A normalization model of attentional modulation of single unit responses. PLoS ONE *4*, e4651.

Lee, D.K., Itti, L., Koch, C., and Braun, J. (1999). Attention activates winner-take-all competition among visual filters. Nat. Neurosci. *2*, 375–381.

Leopold, D.A., and Logothetis, N.K. (1999). Multistable phenomena: changing views in perception. Trends Cogn. Sci. (Regul. Ed.) *3*, 254–264.

Lovejoy, L.P., and Krauzlis, R.J. (2010). Inactivation of primate superior colliculus impairs covert selection of signals for perceptual judgments. Nat. Neurosci. *13*, 261–266.

Machens, C.K., Romo, R., and Brody, C.D. (2005). Flexible control of mutual inhibition: a neural model of two-interval discrimination. Science *307*, 1121–1124.

Marín, G., Salas, C., Sentis, E., Rojas, X., Letelier, J.C., and Mpodozis, J. (2007). A cholinergic gating mechanism controlled by competitive interactions in the optic tectum of the pigeon. J. Neurosci. *27*, 8112–8121.

McPeek, R.M., and Keller, E.L. (2004). Deficits in saccade target selection after inactivation of superior colliculus. Nat. Neurosci. *7*, 757–763.

Müller, J.R., Philiastides, M.G., and Newsome, W.T. (2005). Microstimulation of the superior colliculus focuses attention without moving the eyes. Proc. Natl. Acad. Sci. USA *102*, 524–529.

Mysore, S.P., and Knudsen, E.I. (2011a). Flexible categorization of relative stimulus strength by the optic tectum. J. Neurosci. *31*, 7745–7752.

Mysore, S.P., and Knudsen, E.I. (2011b). The role of a midbrain network in competitive stimulus selection. Curr. Opin. Neurobiol. *21*, 653–660.

Mysore, S.P., Asadollahi, A., and Knudsen, E.I. (2010). Global inhibition and stimulus competition in the owl optic tectum. J. Neurosci. *30*, 1727–1738.

Mysore, S.P., Asadollahi, A., and Knudsen, E.I. (2011). Signaling of the strongest stimulus in the owl optic tectum. J. Neurosci. *31*, 5186–5196.

Naka, K.I., and Rushton, W.A. (1966). S-potentials from luminosity units in the retina of fish (Cyprinidae). J. Physiol. *185*, 587–599.

Niessing, J., and Friedrich, R.W. (2010). Olfactory pattern classification by discrete neuronal network states. Nature *465*, 47–52.

Nummela, S.U., and Krauzlis, R.J. (2010). Inactivation of primate superior colliculus biases target choice for smooth pursuit, saccades, and button press responses. J. Neurophysiol. *104*, 1538–1548.

Ohshiro, T., Angelaki, D.E., and DeAngelis, G.C. (2011). A normalization model of multisensory integration. Nat. Neurosci. *14*, 775–782.

Olsen, S.R., Bhandawat, V., and Wilson, R.I. (2010). Divisive normalization in olfactory population codes. Neuron *66*, 287–299.

Pangratz-Fuehrer, S., and Hestrin, S. (2011). Synaptogenesis of electrical and GABAergic synapses of fast-spiking inhibitory neurons in the neocortex. J. Neurosci. *31*, 10767–10775.

Picardo, M.A., Guigue, P., Bonifazi, P., Batista-Brito, R., Allene, C., Ribas, A., Fishell, G., Baude, A., and Cossart, R. (2011). Pioneer GABA cells comprise a subpopulation of hub neurons in the developing hippocampus. Neuron *71*, 695–709.

Pouille, F., Marin-Burgin, A., Adesnik, H., Atallah, B.V., and Scanziani, M. (2009). Input normalization by global feedforward inhibition expands cortical dynamic range. Nat. Neurosci. *12*, 1577–1585.

Prather, J.F., Nowicki, S., Anderson, R.C., Peters, S., and Mooney, R. (2009). Neural correlates of categorical perception in learned vocal communication. Nat. Neurosci. *12*, 221–228.

Reynolds, J.H., and Heeger, D.J. (2009). The normalization model of attention. Neuron *61*, 168–185.

Reynolds, J.H., Chelazzi, L., and Desimone, R. (1999). Competitive mechanisms subserve attention in macaque areas V2 and V4. J. Neurosci. *19*, 1736–1753.

Sereno, M.I., and Ulinski, P.S. (1987). Caudal topographic nucleus isthmi and the rostral nontopographic nucleus isthmi in the turtle, Pseudemys scripta. J. Comp. Neurol. *261*, 319–346.

Wang, X.J. (2008). Decision making in recurrent neuronal circuits. Neuron *60*, 215–234.

Wang, Y., Major, D.E., and Karten, H.J. (2004). Morphology and connections of nucleus isthmi pars magnocellularis in chicks (Gallus gallus). J. Comp. Neurol. *469*, 275–297.

Williford, T., and Maunsell, J.H. (2006). Effects of spatial attention on contrast response functions in macaque area V4. J. Neurophysiol. *96*, 40–54.

Yang, X.L., and Wu, S.M. (1991). Feedforward lateral inhibition in retinal bipolar cells: input-output relation of the horizontal cell-depolarizing bipolar cell synapse. Proc. Natl. Acad. Sci. USA *88*, 3310–3313.

Neuron, Volume *73*

Supplemental Information

Reciprocal Inhibition of Inhibition: A Circuit Motif for Flexible Categorization in Stimulus Selection

Shreesh P. Mysore and Eric I. Knudsen

SUPPLEMENTAL DATA

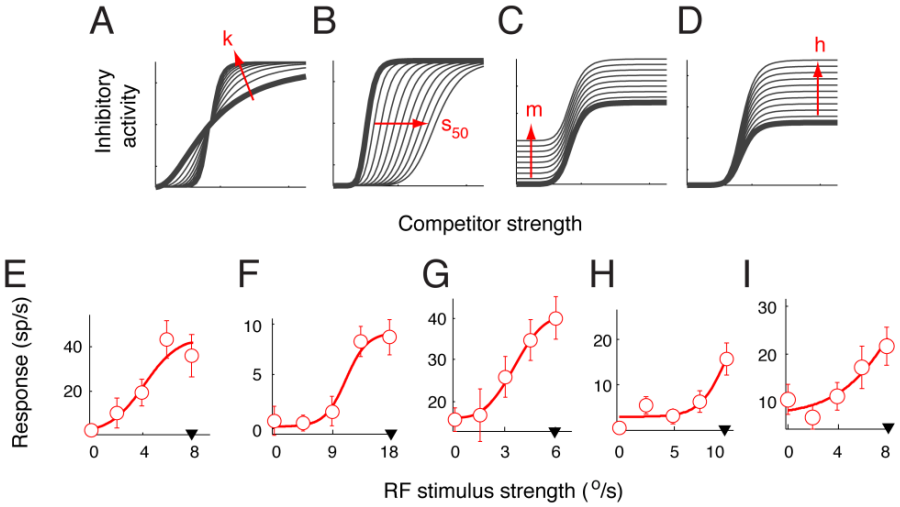

Figure S1 (related to Fig. 2). Strength-response functions for inhibitory units, and effect of RF stimulus strength on scaling of the responses to losing RF stimuli.

(A-D) Strength-response functions for inhibitory units. The plots show the effect of increasing each of the four parameters (eqn. 5) on the shape of the response function of inhibitory unit #2: (A) saturation parameter (k), (B) loom speed at half-max response (S_{50}), (C) minimum response (m), (D) maximum change in response (h). The arrows indicate increasing values of each parameter, while all other parameter values are held constant. Of particular interest are k and S_{50}. Larger values of k result in an increase in the maximum slope (faster approach to saturation) of the sigmoidal function. Larger values of S_{50} result in rightward shifts of the sigmoidal function along with a reduction in the maximum slope (slower approach to saturation). Note: the "competitor" (referred to in the x-axis label) is the competitor stimulus for output unit #1, and therefore, the RF stimulus for inhibitory unit #2. Increasing "competitor" strength, therefore, increases excitatory drive to inhibitory unit #2.

(E-I) Effect of RF stimulus strength on scaling of the responses to losing RF stimuli. When the RF stimulus is weaker than the distant competitor ("losing" RF stimulus), the responses of OTid neurons are not driven to zero. Moreover, if the RF stimulus strength is increased, the responses also increase, rather than remaining fixed, thereby demonstrating that OTid responses are not winner-take-all (Fig. 2E and Mysore et al., 2011). To examine how the responses to a losing RF stimulus scale with its strength, we systematically increased the strength of the RF stimulus over a range of values, while presenting a competitor stimulus of fixed strength such that the RF stimulus was always weaker than the competitor. The resulting responses reveal this scaling, and the results show that the scaling is

typically nonlinear and sigmoidal: Responses measured at five example neurons to varying RF stimulus strength (E-I). The strength of a simultaneously presented competitor stimulus was always greater than that of the RF stimulus (strength indicated graphically by the black arrowhead on the x-axis). Solid lines show best sigmoidal fits to the data. Error bars indicate SEM.

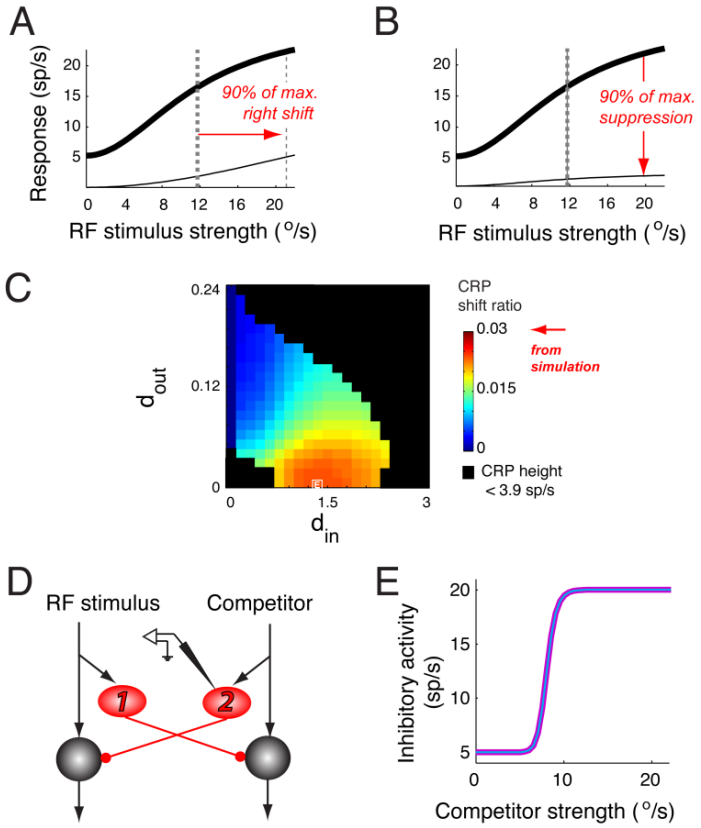

Figure S2 (related to Fig. 3). Range of input (d_{in}) and output (d_{out}) division factors and inhibitory activity during CRP calculations with circuit #1.

(A) Thick line: single stimulus-response function (same as in Fig. 2A). Thin line: the same response function in the presence of a competitor stimulus (loom speed = 8 °/s) exerting a purely input divisive influence of 90% of the maximum (d_{in} = 3). The maximum possible effect was one that shifted the half-max loom speed (L_{50}) from 11.6 to the edge of the relevant range of loom speeds (22 °/s).

(B) Same as in A, except showing a purely output divisive influence of 90% of the maximum (d_{out} = 0.24). The maximum effect was one that suppressed the maximum response rate to 0.

(C) CRP shift ratio (shift in CRP switch value / change in the strength of the RF stimulus) as a function of the input and output division factors (d_{in} and d_{out}), rescaled to show the pattern of variations in shift ratios.

(D) Schematic of the feedforward lateral inhibition model. The recording icon indicates the inhibitory unit for which the output is described in panel E.

(E) Activity of inhibitory unit 2. Thick, magenta line: Inhibitory activity during the calculation of the CRP with the weaker RF stimulus. Thin, blue line: Inhibitory activity during the calculation of the CRP with the stronger RF stimulus (identical to thick, magenta line). The "competitor" (referred to in the x-axis label) is the competitor stimulus for output unit #1, and therefore, the RF stimulus for inhibitory unit #2.

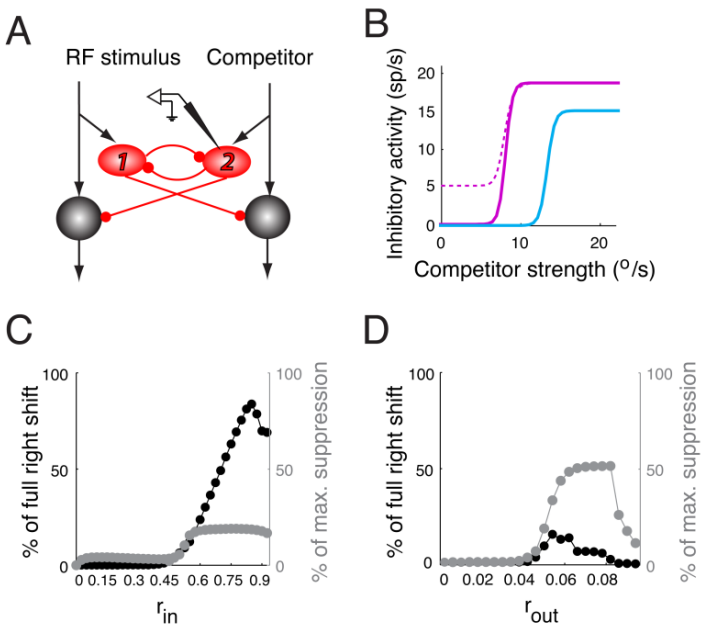

Figure S3 (related to Fig. 4). Steady state inhibitory activity during CRP calculations with circuit #2.

(A) Schematic of the reciprocal inhibition of feedforward lateral inhibition model. The recording icon indicates the inhibitory unit for which the output is described in panels B-D.

(B) Activity of inhibitory unit 2. Solid magenta line: Inhibitory activity during the calculation of the CRP with the weak RF stimulus (8°/s). Dashed magenta line: Reproduction of solid magenta line from Fig. S3E, for comparison. Blue line: Inhibitory activity during the calculation of the CRP with

the stronger RF stimulus (14°/s). r_{in} = 0.84, r_{out} = 0.01. The "competitor" (referred to in the x-axis label) is the competitor stimulus for output unit #1, and therefore, the RF stimulus for inhibitory unit #2.

(C) r_{in} controls the magnitude of the rightward shift of the inhibitory activity (data in black), and, to a lesser extent, contributes to suppression of the inhibitory activity in response to the strongest competitor stimulus (data in gray): Increasing r_{in} led to larger rightward shifts of the inhibitory activity up to a point, beyond which the rightward shifts grew smaller in magnitude (black); the maximum rightward shift was obtained with r_{in} = 0.84. Increasing r_{in} also led to increased response suppression with maximum competitor speed (gray). For these simulations, r_{out} = 0. Rightward shift expressed as a percentage of the full, desired shift (of 6°/s).

(D) r_{out} controls the magnitude of suppression of the inhibitory activity in response to the strongest competitor stimulus (data in gray), and to a lesser extent, contributes to the rightward shift of the inhibitory activity (data in black). Increasing r_{out} led to increased response suppression with maximum competitor speed (gray) and also to small increases in the rightward shift of the inhibitory activity (black). For these simulations, r_{in} = 0.

For B-D, the parameters of the inhibitory response function were chosen to be k=10, S_{50}=8, m=5, and c=15 (same as for all previous figures).

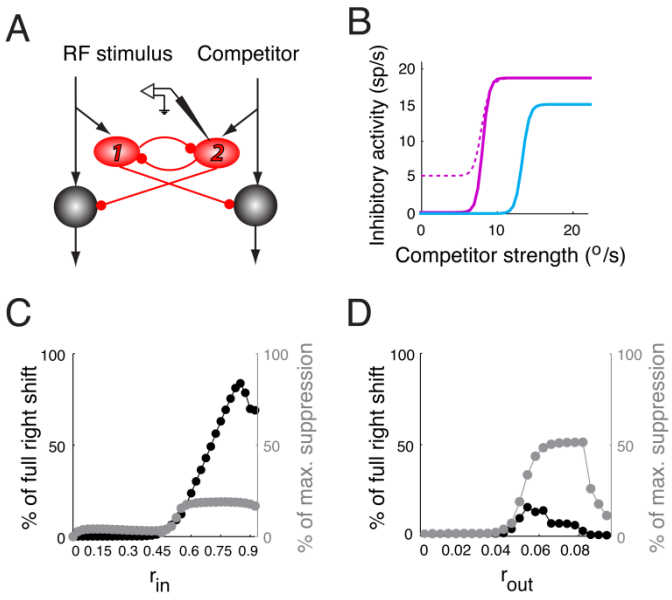

Figure S4 (related to Fig. 5). Effect of the strength of reciprocal inhibition and of parameters of the inhibitory response function on the CRP shift ratio.

(A) CRP shift ratio (shift in CRP switch value / change in the strength of the RF stimulus) as a function of the input and output division factors (d_{in} and d_{out}), rescaled to show the pattern of variations in shift ratios.

(B) CRP shift ratio plotted against r_{in} (left panel) and r_{out} (right panel). Ranges of r_{in} and r_{out} were selected based on Figure S4C,D.

(C) CRP shift ratio plotted as a function of each parameter of the inhibitory response function: saturation, half-max response speed, min response and max response.

For these simulations, the baseline values of the parameters were r_{in} = 0.84, r_{out} = 0.01, k=10, S_{50}=8, m=5, and c=15. The values of one of parameters was varied while the values of the others were held constant at these values. d_{in} = 1 and d_{out}=0.05.

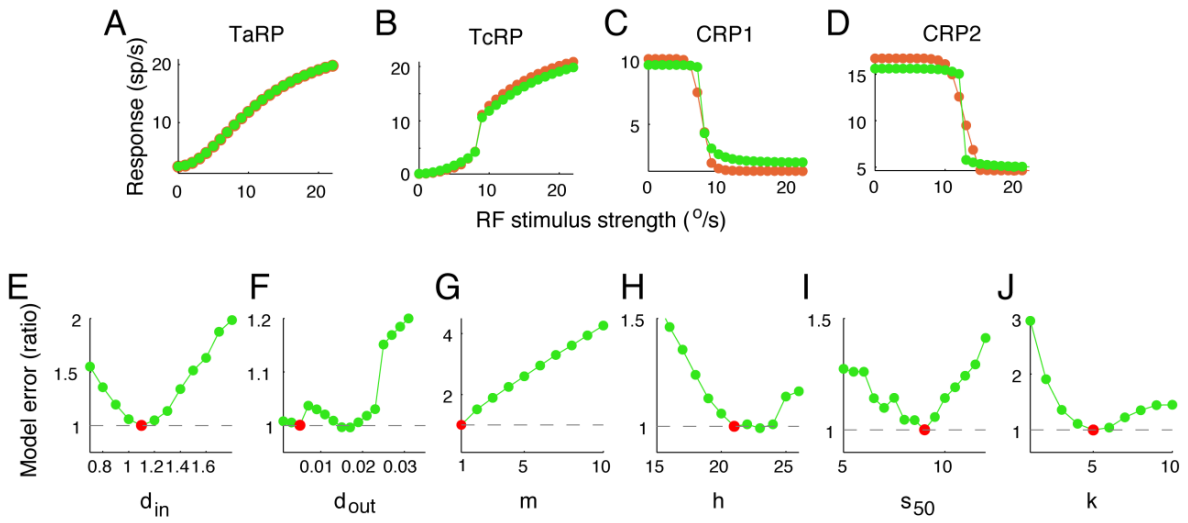

Figure S5 (related to Fig. 7). Choosing parameter values for the circuit with feedback inhibition by the output units.

(A-D) Comparison of the response properties of output unit 1 in the reciprocal inhibition of feedforward lateral inhibition model (circuit #2; Fig. 4) and feedback inhibition by output units model (circuit #3; Fig. 7A). The steady state TaRP (A), TcRP (B), and CRP (C,D) computed by the two models (in orange and green, respectively) are nearly identical. The strengths of the RF stimulus in C and D were 8 °/s and 14 °/s, respectively; the strength of the competitor was 8 °/s. The parameter values of the circuit #2 model were the same as in Figures 5E and 7E-H. The parameters of the circuit #3 model were chosen to be optimal (minimum model error; see panels E through J): d_{in} = 1.1, d_{out} = 0.005, m=1, h=21, S_{50} = 9, and k=5.

(E-J) Error in the responses of output unit 1 in the circuit #3 model versus those in the circuit #2 model, called "model error" (Experimental Procedures), as a function of the values of the parameters of circuit #3. Plotted is the model error ratio, i.e., the model error obtained with a given set of parameter values divided by the error obtained with the optimal set of parameter values. Ratio greater than 1 indicate more error with a given set of parameter values that with the optimal set of parameter values. The parameters of circuit #3 that are systematically varied are: (E) the strength of input division (d_{in}), (F) the strength of output division (d_{out}), and (G-J) the parameters of the inhibitory response functions (m, h, S_{50}, *and* k). The red filled circles indicate the optimal parameter values. Although other values of two of the parameters (d_{out}, panel F; h, panel H) yielded model errors equal to the optimal model error (model error ratio = 1), other aspects of the responses obtained with these parameter values made them a sub-optimal choice. For instance, d_{out} values around 0.015 (F) and h

values between 22 and 24 (H) yielded optimal model error. However, in both cases, the switch value of CRP1 with the circuit #3 circuit was not equal to the switch value of CRP1 with the circuit #2 circuit, unlike when d_{out} and h were optimal (0.005 and 21, respectively; panel C).

For these simulations, the baseline values of the parameters were the same as in panels A-D. The values of one of parameters was varied while the values of the others were held constant at these values.

Table S1 (related to Fig. 6). Values of model parameters used to generate plots in Figure 6A-E.

FIG. 6 PANEL#	d_{in}	d_{out}	r_{in}	r_{out}	**Parameters of response function of excitatory (output) unit**				**Parameters of response function of inhibitory unit**			
					Min. response	***Max. change in response***	L_{50}	***Saturation parameter***	***m***	***h***	S_{50}	***k***
A	1.65	0.12	0.84	0.01	10	25	6.5	2.5	5	15	8	1.8
B	0.25	0.08	0.05	0.01	5	25	8	2.5	5	15	8	1.8
C	1.65	0.12	0.84	0.01	10	25	6.5	2.5	5	15	8	5
D	1.65	0.9	0.84	0.01	5	25	6.5	2.5	5	15	7	5.5
E	1.65	0.32	0.84	0.045	10	14	6.5	9	5	20	7	1.75

SUPPLEMENTAL EXPERIMENTAL PROCEDURES

Computational modeling

Stimulus protocols. Two stimulus protocols were simulated. One protocol generated a competitor strength-response profile or "CRP." In this protocol, the strength of one stimulus (corresponding to the stimulus inside the unit's RF, "RF stimulus") was held at a constant strength (8 °/s), while that of a second stimulus (corresponding to the stimulus outside the RF, "competitor") was varied systematically (0-22°/s). Each stimulus drove a distinct column of excitatory and inhibitory units in the model. The strength of the RF stimulus and the range of strengths of the competitor corresponded to those used previously in experiments (Mysore et al., 2011). When two CRPs were simulated, CRP1 was computed with a fixed RF stimulus strength of 8°/s, and CRP2 was computed with a fixed RF stimulus strength of 14 °/s.

The second stimulus protocol computed responses to increasing strengths of the RF stimulus either alone or in the presence of a competitor with fixed strength (8 °/s). The resulting responses were referred to, respectively, as the "Target-alone response profile" and the "Target-with-competitor response profile".

Pertaining to equation 3: Input divisive inhibition shifts and scales the single stimulus-response function along the horizontal axis of (Fig. 2C, left panel), and was simulated by adding a suppression factor s_{in} to the denominator of the response function in equation 1. Output divisive inhibition controls scaling along the vertical axis (Fig. 2C, right panel), and was simulated by adding a suppression factor s_{out} that scaled the output. We note that in previous models of divisive influences (Cavanaugh et al., 2002; Olsen et al., 2010; Williford and Maunsell, 2006), response firing rates are typically zero for a zero value of the independent variable, such as the contrast of a visual stimulus, or the concentration of an odorant stimulus. However, as described above, the response firing rates to a stimulus with a loom speed of 0 °/s are not zero (on average = 5.3 sp/s; eqn. 2); they represent the response to a stationary dot at full contrast. In order to allow for the input divisive influence to modulate both this contrast-dependent response as well as the loom speed-dependent response, the s_{in} term appears twice in equation 3 unlike in previous models. It appears once for input division of the drive due to stimulus contrast (with an exponent of 1, reflecting the linear dependence of responses on stimulus contrast, c), and a second time for input division of the drive due to stimulus loom (with an exponent of 2, matching the exponent of l; eqn. 3; Olsen et al., 2010).

Neurophysiology

Experimental protocol. Experiments to test the model predictions were performed following protocols that have been described previously (Mysore et al., 2010, 2011). Briefly, epoxy-coated tungsten microelectrodes (FHC, 250um, 1-5 MW at 1kHz) were used to record single and multi-units extracellularly in the OTid of 7 barn owls that typically were tranquilized with a mixture of nitrous oxide and oxygen. Multi-unit spike waveforms were sorted off-line into putative single units (Fee et al., 1996; Mitra and Bokil, 2008). All recordings were made in layers 11-13 of the optic tectum, the intermediate and deep layers of the optic tectum, or OTid.

Stimulus protocol. The looming (expanding) visual stimuli used here and the responses of OTid neurons to looming stimuli have been described elsewhere (Mysore et al., 2010, 2011). Briefly, looming stimuli were full contrast dots that expanded linearly in size over time, starting from a size of 0.6° in radius. Loom speeds were varied within the range of 0 °/s to 22 °/s, determined previously to be the range over which OTid neurons are most sensitive to stimulus loom (Mysore et al., 2010). Note that a stimulus with a loom speed of 0 °/s corresponded to a stationary dot, 0.6º in radius, at full contrast.

Neuronal responses were measured to the simultaneous presentation of two stimuli following the Target-alone response profile/Target-with-competitor response profile protocol. One stimulus, referred to as the RF stimulus, was presented at the center of the RF of the unit, and its strength (loom speed) was varied systematically. The resulting responses yielded the Target-alone response profile. In other measurements, a second stimulus, referred to as the competitor, was presented far outside the RF (30° away), and its strength was held fixed (median loom speed = 8°/s, with a 95% confidence interval of [8 °/s, 12 °/s], n=71). The resulting responses yielded the target (with competitor) strength-response profile (Target-with-competitor response profile).

Data analysis. Response firing rates were computed by counting spikes over a 100 to 250 ms window with respect to stimulus onset, and converting the resulting count into spikes per second. Target-alone response profile (or Target-with-competitor response profile) responses were considered to be correlated with the strength of the RF stimulus when the p-value of the correlation (Spearman's rank correlation coefficient, *corr* command in MATLAB with the Spearman option) was less than 0.05.

The competitor was considered to have a significant effect on neuronal responses when the Target-alone response profile and Target-with-competitor response profile for at least one value of RF stimulus strength were significantly different. For this analysis, responses were compared pair-wise at each strength of the RF stimulus and the resulting p-values were corrected for multiple

comparisons using the Holm-Bonferroni correction. A corrected p-value of less than 0.05 indicated a significant difference.

Sigmoidal functions were fit to the Target-alone response profile and Target-with-competitor response profile for those neurons for which both response profiles were correlated with RF strength and for which the competitor exerted a significant effect. The parameters of the best-fit sigmoids were used to further characterize the nature of the effect of a competitor on Target-alone response profiles.

For all statistical analyses, parametric or non-parametric tests were applied based on whether the distributions being compared were Gaussian or not (Lilliefors test of normality), and corrections for multiple comparisons were applied when appropriate. Data shown as a ± b refer to mean ± s.e.m, unless otherwise indicated.

SUPPLEMENTAL REFERENCES

Fee, M.S., Mitra, P.P., and Kleinfeld, D. (1996). Automatic sorting of multiple unit neuronal signals in the presence of anisotropic and non-Gaussian variability. J Neurosci Methods *69*, 175-188.
Mitra, P., and Bokil, H. (2008). Observed Brain Dynamics (New York: http://www.chronux.org, Oxford University Press).